Published as: Scripta Materialia 155, 2018, Pages 21–25

Achieving ultra-high hardness of nanostructured Mg-8.2Gd-3.2Y-1.0Zn-0.4Zr alloy produced by a combination of high pressure torsion and ageing treatment

W.T. Sun[1], X.G. Qiao[1]*, M.Y. Zheng[1]*, X.J. Zhao[2], H.W. Chen[2], N. Gao[3], M.J. Starink[3]

[1] School of Materials Science and Engineering, Harbin Institute of Technology, Harbin 150001, PR China

[2] College of Materials Science and Engineering, Chongqing University, Chongqing 400044, PR China

[3] Materials Research Group, Faculty of Engineering and the Environment, University of Southampton, Southampton SO17 1BJ, UK

* zhenghe@hit.edu.cn, Tel.: +86 451 86402291, fax: +86 451 86413922

* xgqiao@hit.edu.cn, Tel.: +86 451 86402291, fax: +86 451 86413922

Abstract:

A Mg-8.2Gd-3.8Y-1.0Zn-0.4Zr(wt.%) alloy is subjected to a series of thermal and mechanical treatments involving solution treatment, artificial ageing to peak hardness, high pressure torsion (HPT) and a second artificial ageing. During HPT precipitates dissolve and during the final post-HPT ageing, the supersaturated solid solution decomposes and solutes segregate at grain boundaries. By employing this T6+HPT+T5 treatment, the hardness increases to 156±1 HV, which is much higher than that achieved by any other reported combination of thermal and thermo-mechanical processing of Mg alloys. The ultra-high hardness is due to the combined effects of solute segregation, grain refinement and high dislocation density.

Keywords: Magnesium-rare earth alloy; high pressure torsion; microstructure refinement; ageing response; solute segregation.

Magnesium alloys have potential applications in the fields of aerospace, automobile and electronics owing to their advantages of light weight, high specific strength, and high specific stiffness [1, 2]. In particular, Mg-based alloys containing rare earth (RE) elements are promising candidates for achieving ultra-high strength due to solid solution strengthening and precipitation hardening [3, 4].

Fabrication of bulk ultrafine-grained (UFG) structure by severe plastic deformation (SPD) is an effective way to improve the mechanical properties of Mg-based alloys [5, 6]. High pressure torsion (HPT) is capable of producing a more significant grain refinement and higher dislocation density at room temperature compared to other SPD techniques [7, 8].

Previous studies indicate that the microstructure evolution during HPT is influenced strongly by different heat treatment prior to deformation, such as

solid solution treatment [9] and peak ageing [10]. It was also found that the degree of grain refinement depends strongly on fine coherent precipitates [9-11]. In the Mg-8.2Gd-3.8Y-1.0Zn-0.4Zr(wt.%) alloy, the dense nanosized β′-Mg7RE precipitates introduced by ageing before deformation strongly enhance grain refinement during HPT, and recently a mean grain size of ~33nm has been obtained, which is much finer than other HPT-processed Mg alloys [10]. During HPT processing of this alloy, the β′ phase precipitates are cut by the moving dislocations and gradually dissolve into the α-Mg matrix, resulting in the formation of a supersaturated solid solution, and thus it is expected that a post-HPT ageing treatment will further improve the mechanical properties. This work aims to produce exceptionally high hardness by a combination of HPT processing with ageing treatment using both before and after deformation, and the development of the microstructure is investigated.

The Mg-8.2Gd-3.8Y-1.0Zn-0.4Zr (wt.%) alloy used in this work was produced by direct-chill casting [12], followed by a T6 treatment which involved solution heat treatment at 510 ^{o}C for 12 h and quenching, followed by ageing at 200oC for 48 h. This ageing caused the hardness to increase to ~116 HV due to the formation of fine β′ phase precipitates [13]. Disks with diameter of 10.0mm and thickness of 1.0 mm were cut from the T6-treated alloy and mechanically polished to a final thickness of ~0.85 mm. 16 turns of HPT processing was conducted on these disks at room temperature under quasi-constrained conditions using a pressure of 6.0 GPa. During this processing the β′ precipitates dissolved and a nanostructured supersaturated solid solution with grain size of ~33 nm was achieved [10]. In order to further improve the mechanical properties, re-ageing at a low temperature of 120 ^{o}C was performed on the T6+HPT-processed disk, producing a T6+HPT+T5 treatment. The microstructure of the sample was observed by an FEI TitanG^2 60-300 ChemiSTEM transmission electron microscopy (TEM) equipped with a Super-X EDS detector and operated at 300 kV. The TEM sample was punched at a position 2.5 mm from the center of disk and then mechanically ground and ion milled to perforation. X-ray diffraction was performed using an X'Pert PRO X-Ray diffractometer (XRD) equipped with a graphite monochromator using Cu Kα radiation. The dislocation densities and crystallite sizes of the samples were deduced by analyzing the XRD line profiles via the Materials Analysis Using Diffraction (MAUD) software; details of this procedure were described in [10, 11, 14]. The Vickers hardness was measured using a Zwick microhardness tester under static load of 500 gf for 15 s. Each reported value represents the average of 8 indentations all at the half-radius of the disk. The electrical conductivity, *g*, during ageing was measured using a Sigma 2008B Eddy current conductivity meter.

Fig. 1 shows the age-hardening curve and relative changes of electrical resistivity for the HPT-processed sample during ageing at 120 ^{o}C. The hardness first increases, and reaches a maximum of ~156±1 HV after 10 h, then decreases gradually. This peak-aged hardness is about two times that of the initial cast sample (~77 HV) [11]. The electrical resistivity is mainly determined by the dissolved alloying elements in the α-Mg phase [15]. With increasing ageing time, the electrical resistivity decreases, indicating a continuous reduction in solute concentration of α-Mg matrix during ageing.

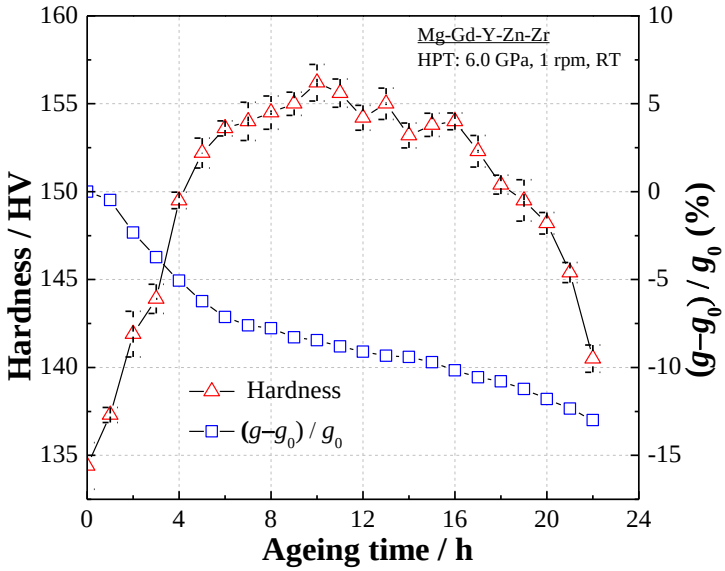

Fig. 1 Age-hardening curve (red triangle) and relative changes of electrical resistivity (g-g_0)/g_0 (blue square) for T6+HPT-processed sample at 120 °C.

Fig.2 shows the microstructure of the T6+HPT+T5-processed Mg-Gd-Y-Zn-Zr alloy after peak ageing. The T6+HPT+T5-processed sample exhibits a nano-grained structure with a mean grain size of 35±2 nm (see Fig. 2(a) and (b)), which is similar to T6+HPT-processed samples [10]. The atomic-resolved HAADF-STEM images and corresponding EDS analysis (see Fig. 2(c)-(f)) show that the concentrations of Gd, Y and Zn atoms along grain boundaries (GBs) and triple junctions are higher than those in the α-Mg matrix, indicating that the solute segregation occurs after post-HPT ageing. There is a strong co-clustering of RE and Zn at triple points. Such solute segregation and clustering will act as obstacles to grain growth and stabilize the nanosized grains by pinning the GBs. Other than these co-clusters, no precipitates are observed.

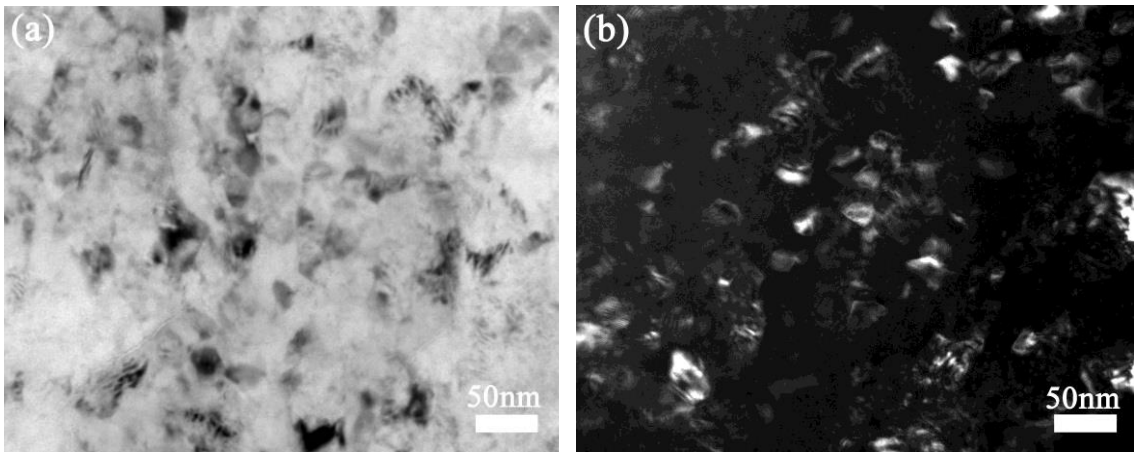

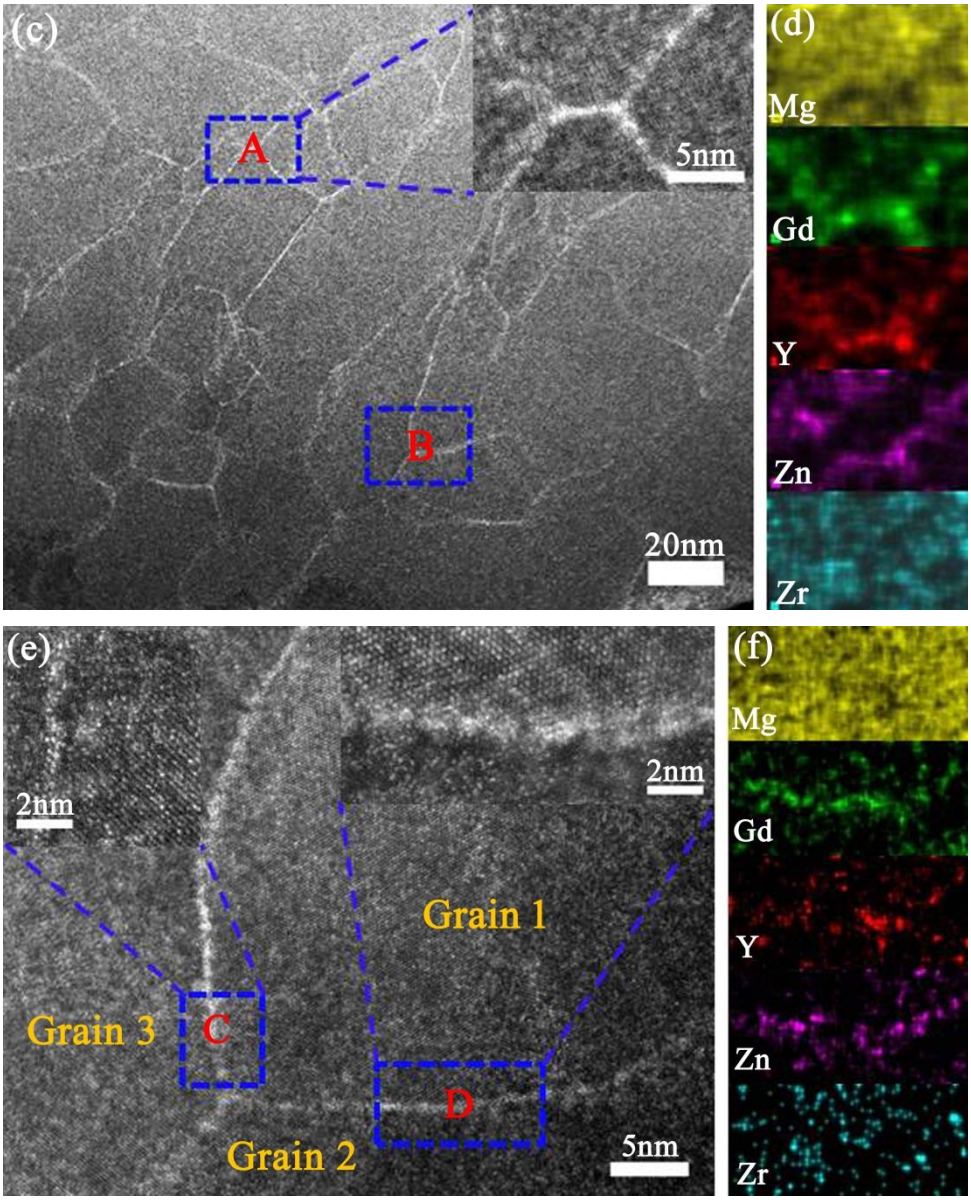

Fig. 2 Microstructure of the T6+HPT +T5-processed Mg-Gd-Y-Zn-Zr alloy at peak ageing: (a) TEM bright-field image; (b) TEM dark-field image; (c) HAADF-STEM image and the inserted high magnification image of area A; (d) corresponding elemental mappings of area A marked in (c); (e) HAADF-STEM image of area B marked in (c) and the inserted high magnification images of areas C and D; (f) corresponding elemental mappings of area D marked in (e).

Fig. 3 shows the XRD patterns of the T6, T6+HPT and T6+HPT+T5-processed Mg-Gd-Y-Zn-Zr samples. After 16 turns of HPT processing only diffraction peaks due to α-Mg phase are detected, suggesting that all the initial precipitates are dissolved and a supersaturated solid solution forms. Careful examination of Fig. 3(b) reveals that in comparison to the as-aged sample the main peaks of α-Mg phase are shifted to lower angle by HPT processing [10], and they shift towards increasing angle with increasing ageing time. The increased lattice parameters after HPT are ascribed to the increased concentration of RE atoms in the α-Mg matrix phase due to the larger size of RE as compared to Mg, while the decreased lattice parameter after post-HPT ageing is due to decomposition of the supersaturated solid solution. In

line with the TEM observations, XRD data also shows no new phase is formed due to ageing. Fig. 3(c) shows that with increasing ageing time, the dislocation density of the HPT-processed sample gradually decreases. The crystallite size of the T6+HPT+T5-processed sample is not significantly changed by the T5 peak-ageing treatment, but it is significantly increased after overageing.

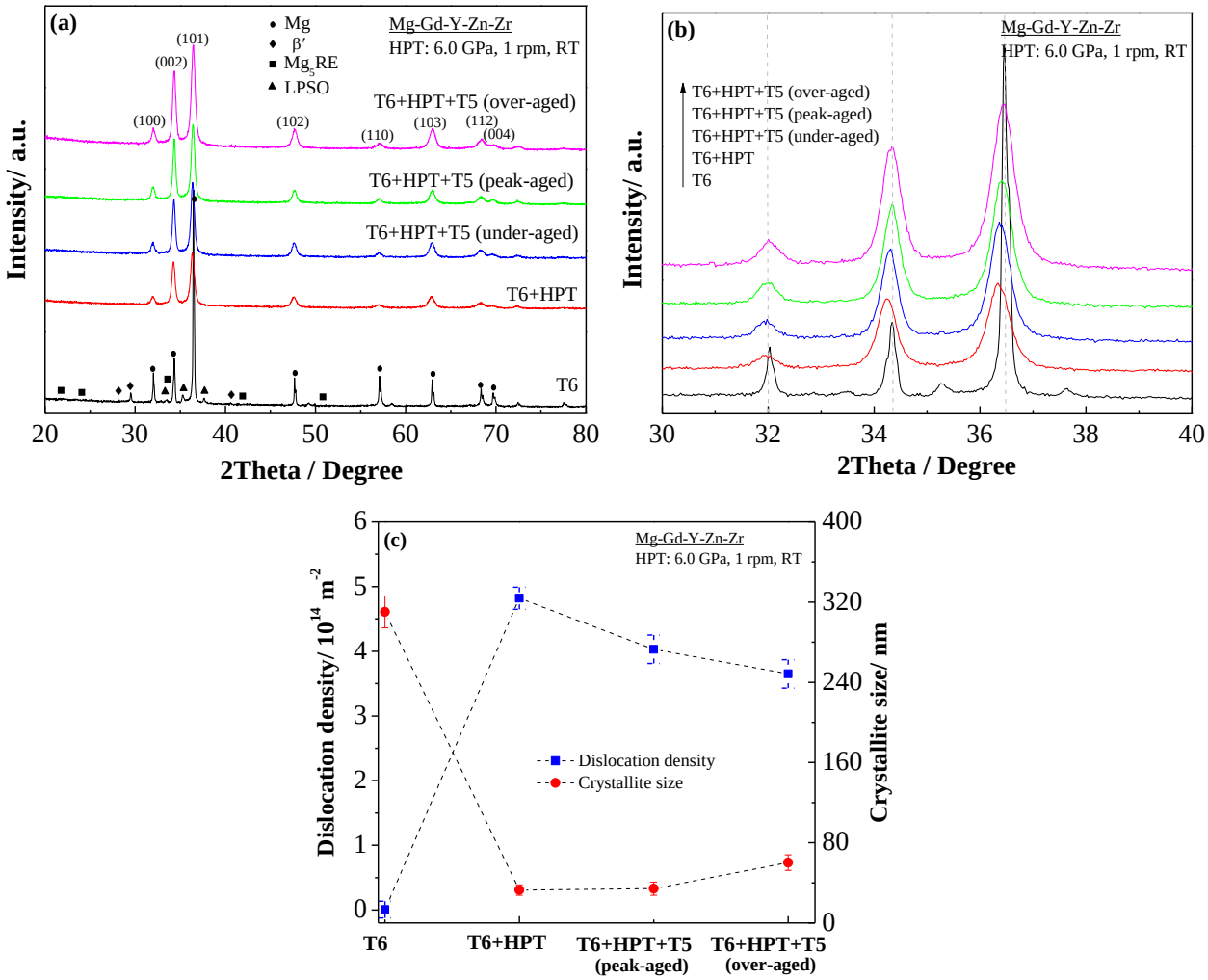

Fig. 3 (a) Overview of XRD patterns of the HPT-deformed and aged Mg-Gd-Y-Zn-Zr alloys; (b) enlarged section of XRD patterns, and (c) the dislocation density and crystallite size at different ageing states.

HPT processing can induce abundant dislocations and significant grain refinement [7, 8]. Fig.1 shows that at the early stages of ageing (t<5 h), the conductivity increases linearly, which suggests that at this stage diffusion towards a linear object (e.g. a dislocation) is the main rate-determining mechanism involved in removal of solutes from the Mg-rich phase. TEM observations in Fig. 2 indicate that with increasing ageing time, some of this removal of solutes proceeds towards the grain boundary. Specific "non-equilibrium" GBs introduced by SPD are associated with excess grain boundary energy, long range elastic stresses and enhanced free volumes [16, 17], which promote solute diffusion, and thus solute segregation can readily occur at these GBs to minimize their local Gibbs free energy. The phenomena of solute

segregation at GBs also occurs in other HPT-processed alloys. For example, in the HPT-processed Al-1Mg-4Cu(wt.%) alloy abundant defects (dislocations, GBs and vacancies) which might stimulate nucleation of semi-coherent S or S′ precipitates were present, but no such precipitates were observed after ageing of the HPT-deformed sample, and instead Cu-Mg clusters dominated the strengthening [18]. These clusters formed at GBs and were detected by atom probe tomography [14]. In an austenitic 316 stainless steel HPT-processed at ambient temperature, post-deformation annealing treatment at 500 °C for 1h caused solute segregation at GBs [19]. It is noted that there is no evidence for the presence of metastable phases in the present peak-aged T6+HPT+T5 Mg-Gd-Y-Zn-Zr alloy. Precipitation sequence modification by skipping the precursor metastable phases during ageing was also observed in various nanostructured Al-Cu alloys processed by severe plastic deformation [20-22].

In our previous research no segregation of solutes at GBs was observed in Mg-Gd-Y-Zn-Zr alloy processed by HPT at ambient temperature [9, 10], but subsequent ageing did induce significant GB segregation. In the present T6+HPT+T5-processed material, the ageing to peak hardness occurs much faster than in the conventionally processed T6-treated Mg-Gd-Y-Zn-Zr material, where 48h at 200oC is required to reach peak hardness [13, 23, 24]. This is thought to be due to the high density of grain boundaries that are available for solutes to segregate to and cluster at, which is a process that unlike precipitate formation does not require the overcoming of an energy barrier associated with a critical nucleus, and thus is faster than classical precipitation. The RE elements have an effective atomic radius larger than Mg whereas the atom radius of Zn is smaller, thus elastic strain energy due to the substantial size misfit between Mg and solutes provides a driving force for the solute segregation at GBs and clustering during ageing. Whilst further analysis (e.g. of entropy effects) is needed, these size effects and their related changes in elastic deformation energy are thought to be the main factors involved in reduction of total free energy in the system at this stage.

We can show that diffusion of the solutes is sufficiently fast to allow significant diffusion of solutes to the grain boundaries in the following way. The temperature-dependent diffusion coefficient D of solutes is estimated by [25]:

$$\mathrm{D} = \mathrm{D}_0 \exp\left(-\frac{\mathrm{Q}}{\mathrm{RT}}\right) \quad (1),$$

where D_0 is a pre-exponential factor, Q is the activation energy, T is the absolute temperature and R is the gas constant. As the diffusion coefficient of Gd is the lowest of the major alloying elements in our alloy [25], Gd diffusion is expected to be the rate-limiting factor for the segregation behavior during ageing. The effective distance of mass transfer approximately equals the diffusion length L, which can be evaluated from [26]:

$$\mathrm{L} = 2\sqrt{\mathrm{Dt}} \quad (2),$$

where t is ageing time. The pre-exponential factor and corresponding activation energy for Gd along the a-axis of the Mg rich phase are 1.27×10^{-9} m^2/s and 79.27 kJ/mol respectively, while along the c-axis the values are 1.79×10^{-9} m^2/s and 81.69 kJ/mol respectively [25, 27]. For Gd diffusion during ageing for 10 h at 120 °C, L is then calculated to be about 60-72 nm, i.e. the diffusion length is similar to (somewhat larger than) the α-Mg matrix grain size of 35±2 nm. In fact, due to the substantial dislocations and vacancies created by HPT, the solute diffusion is expected to be accelerated. This means that at 120 °C the atomic mobility of solutes is sufficient to allow most of them to transport from the grain interiors to the GBs within 10 h, which further indicates that the segregation and clustering of

solutes at the GBs and triples is the key process involved in age hardening in this T6+HPT+T5 treatment.

As shown in Fig. 1, the hardness enhancement caused by post-HPT peak ageing is about 22 HV as compared to the T6+HPT-processed sample. The contributions of refined grains, dislocations and solid solution to hardness can be estimated as follows. The Hall-Petch relationship is used to calculate the grain boundary hardening: $\Delta HV_{GB} = Ck_{HP}d^{-1/2}$, where the d is the mean grain size and k_{HP} is the Hall-Petch coefficient taken as ~40.7 MPa·μm$^{-1/2}$ for Mg [28]. It is considered that in good approximation hardness is proportional to yield strength and the proportionality constant C is taken as 0.3 HV/MPa [29]. The dislocation hardening is described by $\Delta HV_D = CM\alpha_1 Gb\sqrt{\rho_{dis}}$ [30, 31], where M is the Taylor factor, α_1 is a constant equaling 0.3 [30, 31], G is the shear modulus (17.7 GPa for Mg), b is the Burgers vector (0.3197 nm for Mg), and ρ_{dis} is the dislocation density (here obtained from the XRD line broadening analysis) and taken as ~4.8×10^{14} m^{-2} and ~4.0×10^{14} m^{-2} for T6+HPT and T6+HPT+T5 samples respectively (see Fig.3(c)). The solid solution hardening is estimated by the expression $\Delta HV_{SS} = C(\sum k_i^{1/n} c_i)^n$ [32], where c_i are the concentrations of the corresponding solute atoms, n is set as 1/2 and the k_i factors related to individual solute elements are taken as 683 MPa(at.%)$^{-1/2}$, 737 MPa(at.%)$^{-1/2}$, 578 MPa(at.%)$^{-1/2}$ for Gd, Y and Zn, respectively [32]. The T6+HPT-processed sample is a supersaturated solid solution [10], while after peak ageing at 120oC for 10h the solute concentrations in the matrix are close to an equilibrium state, i.e. ~0.05 at.% Gd, ~0.15 at.% Y and 0.002 at.% Zn as obtained from phase diagram [9]. The results for these model predictions are presented in Fig. 4(a), and they show that the hardness contributions from grain size, dislocations and solid solution in the T6+HPT+T5-processed sample are lower than those of the T6+HPT-processed sample by ~2 HV, ~3 HV and ~25 HV respectively. This indicates that the solute segregation at and co-clusters near GBs contribute an increase in the hardness of ~52 HV at the peak aged state.

The peak-age hardness of HPT-processed Mg-RE alloys reported in the literatures [33-37] are summarized in Fig. 4(b). This figure shows that the present processing of Mg-Gd-Y-Zn-Zr alloy, encompassing ageing prior to HPT deformation combined with post-HPT low temperature ageing (i.e.T6+HPT+T5), produces a hardness that substantially exceeds all other reported ones. (And we believe it in fact exceeds *all* hitherto reported hardness values of *all* Mg-based alloys.) This unusually high hardness may be explained by three factors. Firstly, the grain refinement during HPT, enhanced by the presence of fine dispersed precipitates introduced by ageing prior to deformation [10, 38] is producing grains that are smaller than any hitherto reported SPD processing of Mg-RE alloys, in which the starting materials are typically as-cast or solution-treated conditions (see e.g. [33-37]). The HPT-induced re-dissolution of fine precipitates causes super saturation of the α-Mg matrix phase, which plays an important role in the subsequent post-HPT ageing response. It is noted that the larger amount of GBs in the nanostructure will enable increased solute segregation at and co-clustering along GBs after peak ageing. Secondly, in previous reports on HPT-processed and subsequently aged Mg-RE alloys [33-36] the hardness increment is usually attributed to the generation of metastable phases but these works generally did not reliably distinguish and identify the precipitates or solute segregation by TEM observation owing to the nanoscale sizes of the structure constituents and high

dislocation densities. In contrast, for the present HPT-processed Mg-Gd-Y-Zn-Zr alloy, in addition to the contribution of grain refinement to the hardness, the formation of solute segregation after ageing can act as barriers for dislocation movement and thus provide an additional hardening effect, and also improve the thermal stability of nanostructure effectively, leading to an further enhancement of hardness. Thirdly, in the present T6+HPT+T5 treatment the unusually small grains and high dislocation density promote the ageing response, allowing a faster ageing at a lower temperature. The present (T5) treatment at 120 ^{o}C is lower than any other reported ageing temperature to reach peak hardness within a day in a Mg-based alloy. This effectively minimizes recovery (i.e. thermally activated movement and reorganization of dislocations) and thus minimizes hardness reduction due to this process. In addition, the thermal stability of nanograins is improved by the solute segregated at GBs and clustered at triple points, thus limiting the softening effect arising from grain growth. However, as the ageing time increases beyond ~10 h at 120 ^{o}C the hardness decreases. It should be noted that there is nearly no change in the positions of characteristic Mg diffraction peaks between the peak-aged sample and over-aged sample (see Fig. 3(a) and (b)), indicating that the solute segregation at GBs at 120 ^{o}C had completed after 10 h, i.e. the contribution of solute segregation to hardness is similar for the peak aged and the overaged samples. This means that the reduction in hardness during over-ageing is mainly caused by the increasing grain size and decreasing dislocation density (see Fig. 3(c)).

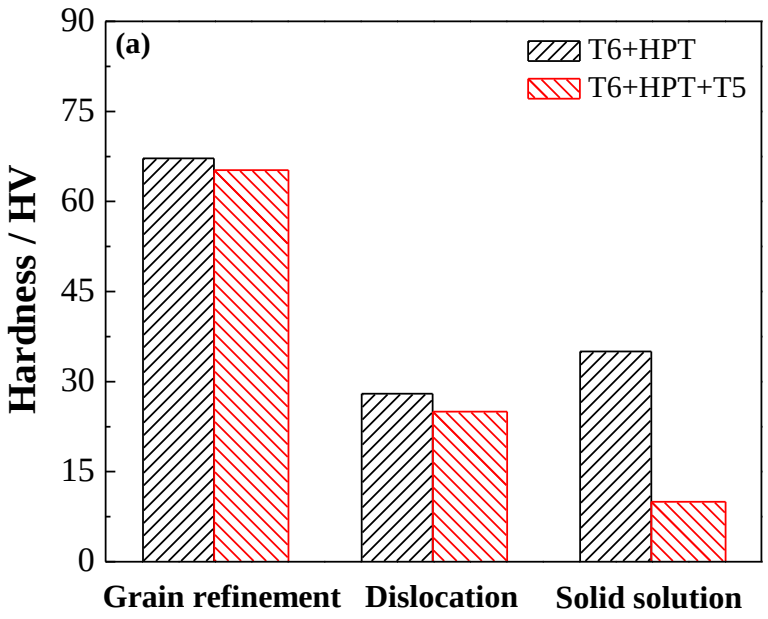

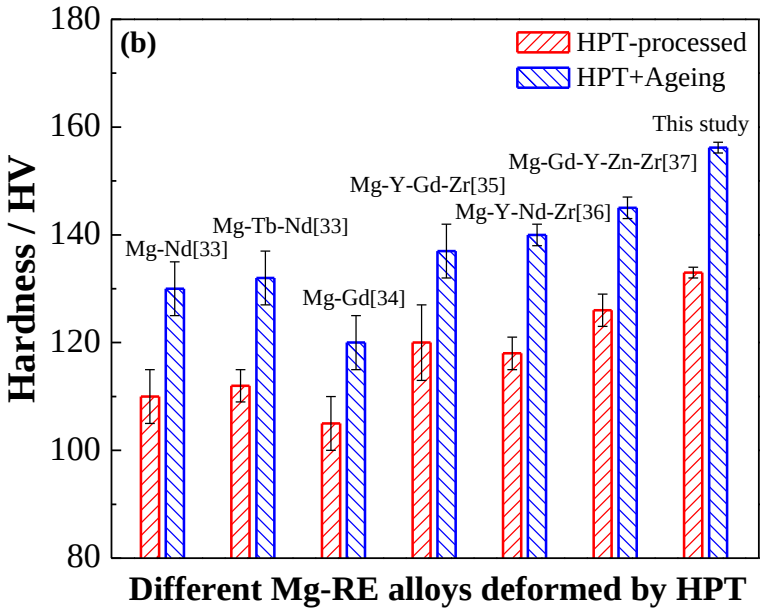

Fig. 4 (a) Contributions of grain refinement, dislocations and solid solution to hardness for T6+HPT-processed and T6+HPT+T5-processed Mg-Gd-Y-Zn-Zr; (b) Comparison of average hardness in different Mg-RE alloys processed by HPT at room temperature and subsequently peak ageing [33-37].

In summary, high pressure torsion at room temperature is performed on a peak-aged Mg-Gd-Y-Zn-Zr alloy, leading to the formation of a supersaturated solid solution with exceptional grain refinement. A record hardness for Mg-based alloys of 156±1 HV is achieved by subsequent post-HPT ageing, which is higher than any Mg- based alloy hitherto reported in the literature. This is attributed to the simultaneous hardening effects from grain refinement, high dislocation density and solute segregation. The generation of solute segregation at grain boundaries enhances thermal stability of the nanostructure during ageing, with an average grain size of ~35 nm at peak-aged stage. The current work provides a feasible approach combining ageing treatments and intense shear deformation to obtain extremely high hardness in nanostructured Mg-RE alloys.

This research was supported by National Natural Science Foundation of China (517 71062 and 51571068).

References

[1] M.K. Kulekci, Int. J. Adv. Manuf. Technol. 39 (2008) 851.
[2] S.H. You, Y.D. Huang, K.U. Kainer, N. Hort, J. Magn. Alloys 5 (2017) 239.
[3] J.F. Nie, Metall. Mater. Trans. A 43A (2012) 3891.
[4] S.H. You, Y.D. Huang, K.U. Kainer, N. Hort, J. Magnesium Alloy 5 (2017) 239.
[5] O.B. Kulyasova, R.K. Islamgaliev, Y.H. Zhao, R.Z. Valiev, Adv. Eng. Mater. 17 (2015) 1738.
[6] A. Singh, D.A. Basha, H. Somekawa, K. Tsuchiya, Scripta Mater. 134 (2017) 80.
[7] A.P. Zhilyaev, T.G. Langdon, Prog. Mater. Sci. 53 (2008) 893.
[8] K. Edalati, Z. Horita, Mater. Sci. Eng. A 652 (2016) 325.
[9] W.T. Sun, X.G. Qiao, M.Y. Zheng, C. Xu, N. Gao, M.J. Starink, Mater. Design 135 (2017) 366.
[10] W.T. Sun, X.G. Qiao, M.Y. Zheng, Y. He, N. Hu, C. Xu, N. Gao, M.J. Starink, Mater. Sci. Eng. A 728 (2018) 115.
[11] W.T. Sun, C. Xu, X.G. Qiao, M.Y. Zheng, S. Kamado, N. Gao, M.J. Starink, Mater. Sci. Eng. A 700 (2017) 312.
[12] C. Xu, M.Y. Zheng, Y.Q. Chi, X.J. Chen, K. Wu, E.D. Wang, G.H. Fan, P. Yang, G.J. Wang, X.Y. Lv, S.W. Xu, S. Kamado, Mater. Sci. Eng. A 549 (2012) 128.
[13] C. Xu, M.Y. Zheng, K. Wu, E.D. Wang, G.H. Fan, S.W. Xu, S. Kamado, X.D. Liu, G.J. Wang, X.Y. Lv, J. Alloys Compd. 550 (2013) 50.
[14] Y. Chen, N. Gao, G. Sha, S.P. Ringer, M.J. Starink,

Acta Mater. 109 (2016) 202.
[15] M.J. Starink, X.M. Li, Metall. Mater. Trans. A 34A (2003) 899.
[16] R.Z. Valiev, R.K. Islamgaliev, I.V. Alexandrov, Prog. Mater. Sci. 45 (2000) 103.
[17] X. Sauvage, G. Wilde, S.V. Divinski, Z. Horita, R.Z. Valiev, Mater. Sci. Eng. A 540 (2012) 1.
[18] J.W. Zhang, N. Gao, M.J. Starink, Mater. Sci. Eng. A 527 (2010) 3472.
[19] H.C. Wang, I. Shuro, M. Umemoto, H.H. Kuo, Y. Todaka, Mater. Sci. Eng. A 556 (2012) 906.
[20] M. Murayama, Z. Horita, K. Hono, Acta Mater. 49 (2001) 21.
[21] N. Tsuji, T. Iwata, M. Sato, S. Fujimoto, Y. Minamino, Sci. Technol. Adv. Mater. 5 (2004) 173.
[22] Y. Huang, J.D. Robson, P.B. Prangnell, Acta Mater. 58 (2010) 1643.
[23] Y.Q. Chi, M.Y. Zheng, C. Xu, Y.Z. Du, X.G. Qiao, K. Wu, X.D. Liu, G.J. Wang, X.Y. Lv, Mater. Sci. Eng. A 565 (2013) 112.
[24] C. Xu, M.Y. Zheng, S.W. Xu, K. Wu, E.D. Wang, G.H. Fan, S. Kamado, X.D. Liu, G.J. Wang, X.Y. Lv, Mater. Sci. Eng. A 559 (2013) 844.
[25] S.K. Das, Y.B. Kang, T.K. Ha , I.H. Jung, Acta Mater. 71 (2014) 164.
[26] W. Xu, D.P. Edwards, X. Wu, M. Stoica, M. Calin, U. Kühn, J. Eckert, K. Xia, Scripta Mater. 68 (2013) 67.
[27] M. Roostaei, M. Shirdel, M.H. Parsa, R. Mahmudi, H. Mirzadeh, Mater. Charact. 118 (2016) 584.
[28] M.J. Starink, X. Cheng, S. Yang, Acta Mater. 61 (2013) 183.
[29] P. Zhang, S.X. Li, Z.F. Zhang, Mater. Sci. Eng. A 529 (2011) 62.
[30] M.F. Ashby, Philos. Mag. 21 (1970) 399.
[31] M.J. Starink, Mater. Sci. Eng. A 705 (2017) 42.
[32] L. Gao, R.S. Chen, E.H. Han, J. Alloys Compd. 481 (2009) 379.
[33] M. VlČek, J. Čížek, O. Melikhova, P. Hruška, I. Procházka, Acta Phys. Pol. A 125 (2014) 744.
[34] O.B. Kulyasova, R.K. Islamgaliev, A.R. Kil'mametov, R.Z. Valiev, Phys. Met. Metallogr. 101 (2006) 585.
[35] S.V. Dobatkin, L.L. Rokhlin, E.A. Lukyanova, M. Yu Murashkin, T.V. Dobatkina, N. Yu Tabachkova, Mater. Sci. Eng. A 667 (2016) 217.
[36] E.A.Lukyanova, N.S. Martynenko, I. Shakhova, A.N. Belyakov, L.L. Rokhlin, S.V. Dobatkin, Yu.Z. Estrin, Mater. Lett. 170 (2016) 5.
[37] W.T. Sun, X.G. Qiao, M.Y. Zheng, C. Xu, S. Kamado, X.J. Zhao, H.W. Chen, N. Gao, M.J. Starink, Acta Mater. 151 (2018) 260.
[38] M.J. Starink, X.G. Qiao, J. Zhang, N. Gao, Acta Mater. 57 (2009) 5796.